Molecular Pharmacology Fast Forward. Published on May 9, 2018 as DOI: 10.1124/mol.117.111047
This article has not been copyedited and formatted. The final version may differ from this version.

The effects of farnesoid X receptor activation on arachidonic acid metabolism, NF-kB signaling and hepatic inflammation

Zhibo Gai, Michele Visentin, Ting Gui, Lin Zhao, Wolfgang E. Thasler, Stephanie Häusler, Ivan Hartling, Alessio Cremonesi, Christian Hiller and Gerd A. Kullak-Ublick*

Department of Clinical Pharmacology and Toxicology, University Hospital Zurich, University of Zurich, Switzerland (Z.G., M.V., S.H., C.H. G.A. K.-U.).

Experiment Center, Shandong University of Traditional Chinese Medicine, Jinan, Shandong, China (T.G.).

Department of Endocrinology, Chinese PLA 309 Hospital, Peking, China (L.Z.).

Department of General and Visceral Surgery, Rotkreuzklinikum Munich, Munich, Germany (W.E.T.).

Department of Clinical Chemistry and Biochemistry, University Children's Hospital Zurich, Switzerland (I.H., A.C.).

Mechanistic Safety, Novartis Global Drug Development, Basel, Switzerland (G.A. K.-U.)

Molecular Pharmacology Fast Forward. Published on May 9, 2018 as DOI: 10.1124/mol.117.111047
This article has not been copyedited and formatted. The final version may differ from this version.

Running Title

FXR and arachidonic acid metabolism.

To whom correspondence should be addressed: Gerd A. Kullak-Ublick, M.D. Department of Clinical Pharmacology and Toxicology, University Hospital Zurich, Rämistrasse 100, CH-8091 Zurich, Switzerland, Telephone: + 41 44 255 2068; FAX: + 41 44 255 9676; E-mail: gerd.kullak@usz.ch

Text pages: 33

Tables: 1

Figures: 7

References: 39

Abstract Word Count: 233

Introduction Word Count: 319

Discussion Word Count: 443

Abbreviations: cytochrome P450, CYP450; dihydroxyeicosatrienoic acids, DHETs; epoxyeicosatrienoic acids, EETs; farnesoid X receptor, FXR; high fat diet, HFD; leukotrienes, LTBs; non-alcoholic fatty liver disease (NAFLD); non-alcoholic steatohepatitis, NASH; obeticholic acid, OCA.

Molecular Pharmacology Fast Forward. Published on May 9, 2018 as DOI: 10.1124/mol.117.111047
This article has not been copyedited and formatted. The final version may differ from this version.

Abstract

Inflammation has a recognized role in non-alcoholic fatty liver disease (NAFLD) progression. The present work studied the effect of high fat diet (HFD) on arachidonic acid metabolism in the liver and investigated the role of the farnesoid X receptor (FXR, NR1H4) in eicosanoid biosynthetic pathways and NF-kB signaling, major modulators of the inflammatory cascade. Mice were fed a HFD to induce NAFLD, then, treated with the FXR ligand obeticholic acid (OCA). Histology and gene expression analysis were performed on liver tissue. Eicosanoid levels were measured from serum and urine samples. The molecular mechanism underlying the effect of FXR activation on arachidonic acid metabolism and NF-kB signaling was studied in Huh7 cells and primary cultured hepatocytes. NAFLD was characterized by higher (~25%) pro-inflammatory (leukotrienes, LTB_4) and lower (~3fold) anti-inflammatory (epoxyeicosatrienoic acids, EETs) eicosanoid levels than in chow mice. OCA induced the expression of several hepatic Cyp450 epoxygenases, the enzymes responsible for EET synthesis, and mitigated HFD-induced hepatic injury. In vitro, induction of CYP450 epoxygenases was sufficient to inhibit NF-kB signaling and cell migration. The CYP450 epoxygenase pan-inhibitor gemfibrozil fully abolished the protective effect of OCA indicating that OCA-mediated inhibition of NF-kB signaling was EET-dependent. In summary non-alcoholic fatty liver disease (NAFLD) was characterized by an imbalance in arachidonate metabolism. Farnesoid X receptor (FXR) activation reprogramed arachidonate metabolism by inducing CYP450 epoxygenase expression and EET

Molecular Pharmacology Fast Forward. Published on May 9, 2018 as DOI: 10.1124/mol.117.111047
This article has not been copyedited and formatted. The final version may differ from this version.

production. In vitro, FXR-mediated NF-kB inhibition, required active CYP450 epoxygenases.

Molecular Pharmacology Fast Forward. Published on May 9, 2018 as DOI: 10.1124/mol.117.111047
This article has not been copyedited and formatted. The final version may differ from this version.

Introduction

The activation of the farnesoid X receptor (FXR, NR1H4), a transcription factor that regulates lipid and glucose metabolism in the liver, reduced hepatic inflammation and fibrosis in a mouse model of non-alcoholic fatty liver disease (NAFLD) (Zhang et al., 2009). Conversely, FXR deficiency caused increased hepatic inflammation and fibrosis (Sinal et al., 2000). FXR activation has been shown to repress NF-kB activation and the production of pro-inflammatory cytokines and pro-fibrotic factors both *in vivo* and *in vitro* (Gai et al., 2016; Hu et al., 2012; Jiang et al., 2007; Miyazaki-Anzai et al., 2010). Arachidonic acid breakdown and metabolism play a major role in triggering and resolving the inflammation. Indeed, the balance between anti-inflammatory (epoxyeicosatrienoic acids, EETs) and pro-inflammatory (leukotrienes, LTBs) arachidonate metabolites is critical in many pathophysiological conditions (Needleman et al., 1986; Zeldin, 2001). Persistent leukotriene B_4 (LTB_4) production is a hallmark of chronic inflammatory diseases, including high-fat diet-induced liver inflammation (Chou et al., 2010; Li et al., 2015a; Samuelsson et al., 1987; Spite et al., 2011; Subbarao et al., 2004; Tager and Luster, 2003). Conversely, High EET levels limit inflammation in cardiovascular disease and metabolic syndrome (Bettaieb et al., 2013; Deng et al., 2010; Imig, 2012; Luria et al., 2011; Sodhi et al., 2012).

EETs are generated from the epoxygenation of arachidonic acid by the cytochrome CYP450 epoxygenases (e.g. CYP2C, CYP2J). CYP450 epoxygenase levels were found decreased in liver of patients with progressive stages of nonalcoholic fatty liver disease (NAFLD), suggesting that CYP450 epoxygenase and EET levels might play a

Molecular Pharmacology Fast Forward. Published on May 9, 2018 as DOI: 10.1124/mol.117.111047
This article has not been copyedited and formatted. The final version may differ from this version.

role in the progression of NAFLD (Fisher et al., 2009). We recently reported that FXR activation induced cytochrome Cyp450 epoxygenase mRNA expression levels in mouse kidney proximal tubular cells (Gai et al., 2016). This work investigated the role of FXR in arachidonate metabolism and characterized the FXR-CYP450-EET interaction in mice with high fat diet (HFD)-induced NAFLD. Finally, we demonstrated in vitro that FXR-mediated NF-kB signaling repression is EET-dependent.

Molecular Pharmacology Fast Forward. Published on May 9, 2018 as DOI: 10.1124/mol.117.111047
This article has not been copyedited and formatted. The final version may differ from this version.

Materials and methods

Animals.

Female C57/BJ mice were randomly assigned to a HFD (D12331; Provimi Kliba, Switzerland) or a chow diet (D12329, Provimi Kliba) for 16 weeks. In a separate experiment, after 8 weeks of a HFD, half the obese mice were given OCA mixed into the food (25 mg/kg, Intercept Pharmaceuticals, NY, USA). Finally, mice were divided into three groups of six animals each: chow, HFD and HFD-OCA. Liver from each animal was used for RNA, protein extraction and histological examination.

Enzyme and metabolite measurements.

For 24h urine collection metabolic cages were employed. Urine and serum 14,15 dihydroxyeicosatrienoic acid (14,15-DHET) levels were measured by ELISA (ab175811, Abcam, Cambridge, UK). Serum triglycerides (TG), alanine aminotransferase (ALT), LTB_4 levels and 14,15-EET levels were measured with a triglyceride assay kit (ETGA-200, EnzyChrom), an ALT assay kit (ab105134, Abcam), a LTB_4 Parameter Assay Kit (KGE006B, R&D systems) and a 14,15-EET ELISA kit (DH2R, Detroit R&D), respectively. EETs and LTB_4 levels in the culture medium were also assessed by UPLC-MS/MS.

Sample preparation for UPLC-MS/MS metabolite analysis.

Five hundred µl of cell culture medium was mixed with 300 µl methanol and 300 µl of ultrapure water. Deuterated LTB_4 and 14,15-EET (d_4-LTB4, d_{11}-14,15-EET; Cayman

Molecular Pharmacology Fast Forward. Published on May 9, 2018 as DOI: 10.1124/mol.117.111047
This article has not been copyedited and formatted. The final version may differ from this version.

Chemical) were added as internal standards. The samples were incubated on ice then centrifuged for 10 min at 1200 x g at 4 °C. The supernatant was collected and diluted 3:1 with 1% NH_4OH then loaded onto a mixed mode solid phase extraction (SPE) column (Evolute Express AX, Biotage). The columns were preconditioned with 1 ml of methanol and 1 ml of 1% NH_4OH. After sample loading, the column was washed with 2 ml 0.5 M ammonium acetate/methanol (95:5) and 2 ml methanol. Analytes were eluted in 6 ml methanol/formic acid (98:2). The eluate was dried under nitrogen at 40 °C, was reconstituted in 30% methanol and injected into a UPLC-MS/MS system.

UPLC-MS/MS analysis of metabolites.

The UPLC-MS/MS method was adapted and modified from Weiss *et al.* (Weiss et al., 2013). Analytes were separated on a CSH C18 column (Acquity UPLC CSH C18 1.7 µm, 2.1 x 150 mm; Waters AG) thermostated at 35 °C using an UPLC (Nexera X2, Shimadzu Schweiz GmbH). Mobile phase A and B consisted of 0.125% NH_4OH in double distilled water and methanol:acetonitrile (70:30), respectively. The following gradient was used; T_0: 35% B, T_2: 35% B, T_4: 42% B, $T_{5.5}$: 44% B, T_7: 52% B, $T_{10.5}$: 52%, T_{14}: 70% B. Mobile phase B was then increased to 90% for 2 min to clean the column before returning to starting conditions for 2 min. Analytes were detected using a Sciex Triple Quad 6500+ mass spectrometer (AB SCIEX GmbH) in negative ion mode and scheduled multiple reaction monitoring (MRM). The optimized MS parameters were as follows: curtain gas (CUR) = 35, collision gas (CAD) = 9, ion spray voltage (IS) = -4500 V, temperature (TEM) = 600 °C, ion source gas 1 (GS1) = 70, ion

Molecular Pharmacology Fast Forward. Published on May 9, 2018 as DOI: 10.1124/mol.117.111047
This article has not been copyedited and formatted. The final version may differ from this version.

source gas 2 (GS2) = 70, declustering potential (DP) = -40 V, entrance potential (EP) = -10 V, cell exit potential (CXP) = -15 V. The MRM transitions used for quantification were 335.3→195.2 for LTB_4, 339.0→197.0 for LTB_4-d_4, 319.1→219.1 for 14,15-EET, and 330.2→219.1 for 14,15-EET-d_{11}. The collision energy was optimized for each analyte as follows; LTB_4 and LTB_4-d_4 = -22 V, 14,15-EET = -16 V, and 14,15-EET-d_{11} = -18 V.

Liver pathological assessments and immunostaining.

Livers were fixed overnight in formalin and embedded in paraffin. Three µm sections were stained with hematoxylin and eosin (HE) and Masson's trichrome stains. The fibrotic areas were determined from the Masson's trichrome stained sections by digital images analyzed by an unbiased observer. Immunostaining was performed on paraffin sections using a microwave-based antigen-retrieval technique. The antibodies used in this study were against CD4 (sc-7219, Santa Cruz), aSMA (NBP1-30894, Novus Biologicals), MAC387 (ab22506, Abcam). Sections were treated with the Envision$^+$ DAB kit (Produktionsvej 42, Dako) according to the manufacturer's instructions.

For NAFLD score analysis, histopathologic damage was scored using the system proposed by the NASH Clinical Research Network. Three representative areas were scored in each section and the average values were used as the final score.

Isolation of RNA from liver tissue and cells and quantification of transcript levels.

Total RNA was prepared using standard Trizol extraction (Invitrogen). Two µg total

Molecular Pharmacology Fast Forward. Published on May 9, 2018 as DOI: 10.1124/mol.117.111047
This article has not been copyedited and formatted. The final version may differ from this version.

RNA were reverse transcribed using random primers and Superscript II enzyme (Invitrogen). First-strand complementary DNA was used as the template for real-time polymerase chain reaction analysis with TaqMan master mix and primers (Applied Biosystems). Data were calculated and expressed relative to levels of RNA for the housekeeping gene hypoxanthine phosphoribosyltransferase (Hprt) or β-actin.

Microarray and gene expression analysis.

RNA was extracted from mouse liver using an RNeasy Microarray Tissue Mini Kit (73304, Qiagen), followed by on-column DNase digestion to remove any contaminating genomic DNA. RNA samples from four mice per group were subjected to microarray analysis. Details on the analysis methods can be found at http://fgcz-bfabric.uzh.ch/wiki/tiki-index.php?page=app.two_groups. Gene ontology analysis, network analysis, and KEGG pathway analysis of the microarray data were completed using the MetaCore online service (Thomson Reuters, https://portal.genego.com/), and DAVID Bioinformatics Resources 6.8 (National Institute of Allergy and Infectious Diseases, NIH, https://david.ncifcrf.gov/).

Cell lines.

Huh7 and THP-1 cells were maintained in RPMI 1640 medium supplemented with 10% fetal calf serum (FCS), 100 units/ml penicillin, 100 μg/ml streptomycin at 37°C in a humidified atmosphere of 5% CO_2. THP-1 cells were supplemented with 2mM L-Glutamine. J774 cells were grown in Dulbecco's modified Eagle's medium (DMEM)

Molecular Pharmacology Fast Forward. Published on May 9, 2018 as DOI: 10.1124/mol.117.111047
This article has not been copyedited and formatted. The final version may differ from this version.

supplemented with 10% FCS, 100 units/ml penicillin, 100 μg/ml streptomycin at 37°C in a humidified atmosphere of 5% CO_2.

Isolation of primary cultured mouse hepatocytes.

Primary culture of hepatocytes were isolated from female C57/BJ mice. After a midline incision, a sterile cannula was inserted through the right ventricle and pre-perfusion was performed at 37°C with pre-perfusion buffer (0.5 mM EGTA, 20 mM Hepes in Hank's Balanced Salt (HBS) solution, pH 7.4) for 10 min. The pre-perfusion buffer was then replaced with perfusion buffer (20 mM $NaHCO_3$, 0.5 mg/ml BSA, 6.7 mM $CaCl_2$, 100 U/ml type II collagenase, in HBS, pH 7.4) for 7 min. The perfused liver was excised, rinsed in ice cold WME-a medium (Williams Medium E with 10% FCS, 2mM L-Glutamine, 2.5 mU/ml Insulin, 1μM Dexamethasone), and gently disaggregated. After centrifugation, cells were counted and tested for viability and cultured at 37°C. After 3 h incubation, WME-a medium was replaced with WME-b medium (Williams Medium E with 10% FCS, 2mM L-Glutamine, 0.25m U/ml Insulin, 0.1μM Dexamethasone).

Isolation of primary cultured human hepatocytes.

Primary human hepatocytes (PHH) were prepared as previously described (Lee et al., 2014) and seeded in six-well plates in hepatocyte maintenance medium supplemented with UltraGlutamine for approximately 5h before further treatment procedures. PHHs were cultured at 37 °C in a humidified atmosphere containing 5% CO_2.

Molecular Pharmacology Fast Forward. Published on May 9, 2018 as DOI: 10.1124/mol.117.111047
This article has not been copyedited and formatted. The final version may differ from this version.

Transient transfection.

Huh7 cells were transiently transfected with pCMV6-Cyp2c29 vector (MR20784, OriGENE). Cells were grown until 80% confluent in 6-well plates then transfected using Fugene HD (Promega) transfection reagent and Opti-MEM (Gibco), according to the manufacturer's protocol. Forty-eight hours after transfection, the cells were treated with the desired experimental conditions.

Migration assay.

Huh7 cells or primary cultured human hepatocytes were seeded on 12-well plates at a density of 0.5 x 10^4 cells/well and then treated with the indicated conditions. After 48-72 hours, 3 µm pore polycarbonate membrane inserts (Costar Corning) were mounted on the wells, seeded with THP-1 cells and incubated for 2h at 37°C. The inserts were washed, fixed and stained with crystal violet for analysis. The medium in which Huh7 cells were grown was collected for LTB_4, EET and DHET content assessment; total RNA was extracted from cells for Real Time PCR analysis. For the migration assay with primary cultured mouse hepatocytes, J774 mouse cells were employed as monocyte-like cells.

Statistics.

Data are expressed as mean ± SD. For microarray data, comparison was assessed by student's *t* test with R/Bioconductor 3.6 (https://www.bioconductor.org/) to generate differentially expressed genes (Chow vs. HFD). For other data relating to baseline

Molecular Pharmacology Fast Forward. Published on May 9, 2018 as DOI: 10.1124/mol.117.111047
This article has not been copyedited and formatted. The final version may differ from this version.

characteristic analysis and histological analysis, comparisons between groups were assessed by either student's *t* test or one-way ANOVA followed by Tuckey's. Statistical comparisons were performed using GraphPad Prism (version 5.0 for Windows, GraphPad Software).

Study approval.

All animal experiments and protocols conformed to the Swiss animal protection laws and were approved by the Cantonal Veterinary Office (study number 2012058). The human study was conducted according to the Declaration of Helsinki guidelines regarding ethical principles for medical research involving human subjects. All patients provided written informed consent, and the study protocol was approved by the Scientific Ethical Committee of Peking University, Beijing, China, where patients were based (license number PKU2010034). Primary human hepatocytes (PHH) were isolated by Human Tissue and Cell Research (HTCR) Foundation upon written informed consent from the patient. The study was approved by the Ethics Committee of the Medical Faculty of the Ludwig Maximilians University (approval number 025-12), in compliance with the Bavarian Data Protection Act.

Results

HFD-induced hepatic inflammation is characterized by decreased expression of cytochrome P450 epoxygenases.

Molecular Pharmacology Fast Forward. Published on May 9, 2018 as DOI: 10.1124/mol.117.111047
This article has not been copyedited and formatted. The final version may differ from this version.

Mice fed a HFD for 16 weeks displayed a higher degree of hepatic lipid deposition and fibrosis than chow mice (Supplementary Fig. 1A and 1B). A NAFLD activity score (NAS) ≥5 is consistent with a diagnosis of non-alcoholic steatohepatitis (NASH). NAS from the liver of HFD mice was ≥5 (Supplementary Fig. 1C).

The arachidonic acid metabolism pathway was markedly changed in the liver from mice fed a HFD (Table 1). The mRNA levels of cytosolic phospholipase A2 (Pla2g) and Alox5, the first committed steps in LTB_4 synthesis pathway, were higher ($P<0.05$) in the liver of HFD mice compared with that of chow mice (Fig. 1A and B). Serum LTB_4 was increased as well in the HFD group as compared with the chow group (Supplementary Fig. 2A). Our data are consistent with a recent study demonstrating an increased hepatic expression of genes associated with eicosanoid synthesis in both diet- and genetic NAFLD mouse models (Hall et al., 2016). Hepatic EET synthesis and degradation in mammalian species are catalyzed mainly by CYP2C epoxygenases and epoxide hydrolase 2 (EPHX2), respectively (Spector and Norris, 2007). The expression of several Cyp2c genes was decreased ($P<0.05$) in the liver of HFD mice compared with that of chow mice (Fig. 1A and B and Table 1). In contrast, the mRNA level of Ephx2, which hydrolyzes EETs to the inactive dihydroxyeicosatrienoic acids (DHETs), was markedly higher than that in the liver of chow mice (Fig. 1B). The concomitant downregulation of several Cyp2c genes and upregulation of Ephx2 resulted in decreased serum 14,15-EET levels and increased urine 14,15-DHET levels in the HFD group in comparison with the chow group (Supplementary Fig. 2B and C). Overall, HFD mice were characterized by an imbalance of arachidonate metabolism

Molecular Pharmacology Fast Forward. Published on May 9, 2018 as DOI: 10.1124/mol.117.111047
This article has not been copyedited and formatted. The final version may differ from this version.

towards inflammation. The expression of canonical genes involved in inflammation and fibrosis strongly correlated with that of EET-related genes in HFD mice (Fig. 1C). Notably, the mRNA level of CYP2C8, one of the major epoxygenases in human liver, was decreased as compared with that from non-NAFLD patients ($P<0.05$) (Fig. 1D). A negative correlation between CYP2C8 mRNA levels and NAFLD score was observed (Fig. 1E). The present data suggest that the expression level of genes involved in EET metabolism and, in turn, EET levels, might regulate the hepatic expression of inflammatory cytokines. Indeed EET treatment could reduce the synthesis of pro-inflammatory cytokines (Li et al., 2015b).

Obeticholic acid induces CYP450 epoxygenase expression and protects the liver from inflammation in vivo.

The impact of FXR activation on arachidonic acid metabolism and on the progression of HFD-induced hepatic inflammation was evaluated. HFD+OCA group showed a reduction in (i) hepatic lipid accumulation, (ii) serum ALT levels, (iii) inflammation, (iv) fibrosis, as compared with the HFD group (Fig. 2 and Supplementary Fig. 3).

The arachidonate metabolism gene expression pattern was markedly changed by FXR activation (Fig. 3A). Alox5 was not affected by OCA treatment (Fig. 3C), but Cyp2c29, one of the main epoxygenase in mouse liver, was induced by OCA treatment ($P<0.05$) (Fig. 3D). mRNA levels of phospholipase A2 and Ephx2, induced by HFD, were restored to the levels of the chow mice by OCA ($P<0.05$) (Fig. 3B and E). Serum LTB_4 levels were increased in HFD mice ($P<0.05$) (Fig. 3F). Serum 14,15-EET levels were

Molecular Pharmacology Fast Forward. Published on May 9, 2018 as DOI: 10.1124/mol.117.111047
This article has not been copyedited and formatted. The final version may differ from this version.

decreased in obese mice (P<0.05) (Fig. 3G). Similarly, urine 14,15-DHET were increased in HFD mice (P<0.05) (Fig 3I). 14,15-EET and 14,15-DHET levels in the HFD+OCA group resembled those in the chow group, in line with the induction of several Cyp2c and the downregulation of Ephx2 mRNA levels. Overall, serum LTB_4/EET index, increased by HFD, was lowered by OCA to the level of the chow mice (P<0.05) (Fig. 3H). Overall OCA could fine tune the arachidonic acid metabolism by reducing LTB_4 levels and inducing EET levels.

FFA-induced monocyte migration in vitro depends on CYP450 epoxygenase activity.

To characterize the interaction between CYP450 epoxygenase and OCA, migration assays were performed in vitro. OCA at an extracellular concentration of 2 μM activated FXR in Huh7 cells (Supplementary Fig. 4). The migration induced by FFA was completely abolished by co-incubation with OCA (P<0.05) (Fig. 4A and B). FFA-induced migration was associated with higher LTB_4 levels in the culture medium as compared with that from the untreated cells and those co-exposed to FFA and OCA (P<0.05) (Fig. 4C). Interestingly 14,15 EET levels were not affected by FFA treatment, but Huh7 cells exposed to OCA showed higher levels of 14,15-EETs in the medium (P<0.05) (Fig. 4D). Overall the ratio of LTB_4/14,15-EETs was markedly decreased in the medium of cells co-treated with FFA and OCA as compared with that in FFA treated cells (P<0.05) (Fig. 4E). 14,15-DHET levels in the culture medium were not changed among the different treatments (Fig. 4F), indicating the changes of 14,15 EET levels were not due to an increased degradation via EPHX2. Along with this, the mRNA level

Molecular Pharmacology Fast Forward. Published on May 9, 2018 as DOI: 10.1124/mol.117.111047
This article has not been copyedited and formatted. The final version may differ from this version.

of CYP2C8, one of the main CYP450 epoxygenases in human liver, was induced by OCA treatment ($P<0.05$) (Fig. 4G). Similar results were obtained using primary cultured hepatocytes from mouse (Supplementary Fig. 5A and B) and human (Supplementary Fig. 5C and D). The protective effect of OCA was fully abolished by the co-incubation with z-Guggulsterone (Gu), a FXR antagonist, ruling out any potential off-target effect of OCA on hepatocytes (Supplementary Fig. 6). The lack of protection by OCA when THP-1 cells were exposed to exogenous LTB_4 indicates that OCA inhibited migration by modulating the synthesis of eicosanoids and not by altering the downstream signaling pathway (Supplementary Fig. 7).

When Huh7 cells were co-incubated with FFA and benzoxathiole derivative (BOT), a NF-κB inhibitor (Kim et al., 2008), FFA-induced THP-1 migration was completely abolished, suggesting that FFA-induced inflammation was NF-κB dependent (Fig. 5A). EETs can suppress NF-κB signaling as well (Dai et al., 2015). In fact, induction of CYP2C gene expression levels in Huh7 cells by pre-treatment with rifampicin, a FXR-independent pan-inducer of CYP2C epoxygenases (Raucy et al., 2002), or by transfection of Cyp2c29, abolished FFA-induced THP-1 cell migration (Fig 5B and C) as well as FFA-induced NF-κB signaling (Fig 5D to G).

It is possible that the inhibitory effect of FXR activation on NF-κB-induced inflammation is EET-dependent. To address this issue, Huh7 cells were co-incubated with FFA, OCA and gemfibrozil (GM), a pan-inhibitor of CYP2C activity (Shitara et al., 2004; Wen et al., 2001). GM abolished the effect of OCA on arachidonate metabolite synthesis

Molecular Pharmacology Fast Forward. Published on May 9, 2018 as DOI: 10.1124/mol.117.111047
This article has not been copyedited and formatted. The final version may differ from this version.

and on THP-1 migration induced by FFA (Fig. 6). Overall, these results indicate that the inhibitory effects of FXR activation on NF-κB signaling was EET-dependent.

Discussion

In the present study, mice fed a HFD displayed an inflammatory and fibrotic pattern compatible with NASH which strongly correlated with a switch in the expression pattern of arachidonate-partitioning genes, notably the downregulation of a number of Cyp2c enzymes which epoxygenate arachidonic acid to EETs, and upregulation of the Ephx2 which inactivates EETs to DHETs (Capdevila et al., 1990; Chacos et al., 1983). As a result, mice fed a HFD were characterized by a dramatic increase in the LTB_4/EET ratio. Arachidonic acid breakdown and LTB_4 formation is known to drive hepatic inflammation (Martinez-Clemente et al., 2010). The present data suggests that EETs are also important in the inflammatory process and may serve as a quencher of LTB_4 signal, buffering the inflammation. The reduced quenching capacity of mice fed a HFD is likely to “unleash” the inflammatory signal produced by the resident macrophages.

OCA treatment elicited less hepatic steatosis, lower expression of pro-inflammatory cytokines and less macrophage infiltration. OCA treatment reprogrammed arachidonate metabolism by inducing Cyp450 epoxygenase expression and downregulating phospholipase A2. These adjustments channeled arachidonic acid into EET synthesis. By boosting EET synthesis, OCA increase the buffering capacity of the liver, and antagonize the inflammatory process. Furthermore, mice fed a HFD and treated with OCA showed a reduced expression of Ephx2 which further contributed to

Molecular Pharmacology Fast Forward. Published on May 9, 2018 as DOI: 10.1124/mol.117.111047
This article has not been copyedited and formatted. The final version may differ from this version.

sustain higher levels of EETs. The anti-inflammatory effect of OCA in vitro was fully abolished by co-incubation with the FXR inhibitor z-Guggulsterone, suggesting that OCA regulated the arachidonic acid pathway via FXR activation with no off-target effects (e.g. TGR5 activation). As FXR activation was reported to modulate macrophage activity, resident macrophages may also respond to the treatment with OCA and contribute to anti-inflammatory effect (McMahan et al., 2013; Verbeke et al., 2016).

Independent studies have shown that both EETs and FXR inhibit the NF-kB pathway (Carroll et al., 2006; Xu et al., 2010; Yang et al., 2007). However when the CYP450 epoxygenase activity was inhibited, OCA could not inhibit NF-kB signaling, suggesting that CYP450 epoxygenase activity is a precondition for FXR-mediated repression of NF-kB signaling (Fig. 7).

To conclude, the induction of CYP450 epoxygenase expression and EET levels is a novel feature of FXR activation and is required for the FXR-mediated NF-kB signaling repression. EET analogs have been reported to attenuate adipogenesis, insulin resistance and inflammation in the adipose tissue of obese mice (Li et al., 2015a; Sodhi et al., 2012; Spite et al., 2011; Zha et al., 2014). Thus, restoring the proper levels of EETs is likely to be beneficial in NAFLD management as well. The induction of endogenous EET levels may contribute to the protective effect of obeticholic acid observed in NAFLD in the clinical setting.

Molecular Pharmacology Fast Forward. Published on May 9, 2018 as DOI: 10.1124/mol.117.111047
This article has not been copyedited and formatted. The final version may differ from this version.

Authors' contribution:

Participated in research design: Gai, Visentin and Kullak-Ublick.

Conducted experiments: Gai, Visentin, Gui, Zhao, Thasler, Häusler, Hartling, Cremonesi, Hiller.

Performed data analysis: Gai, Visentin, Gui, Zhao, Hartling, Cremonesi.

Wrote or contributed to the writing of the manuscript: Gai, Visentin, Hartling, Kullak-Ublick.

Molecular Pharmacology Fast Forward. Published on May 9, 2018 as DOI: 10.1124/mol.117.111047
This article has not been copyedited and formatted. The final version may differ from this version.

References

Bettaieb A, Nagata N, AbouBechara D, Chahed S, Morisseau C, Hammock BD and Haj FG (2013) Soluble epoxide hydrolase deficiency or inhibition attenuates diet-induced endoplasmic reticulum stress in liver and adipose tissue. *J Biol Chem* **288**(20): 14189-14199.

Capdevila JH, Falck JR, Dishman E and Karara A (1990) Cytochrome P-450 arachidonate oxygenase. *Methods in enzymology* **187**: 385-394.

Carroll MA, Doumad AB, Li J, Cheng MK, Falck JR and McGiff JC (2006) Adenosine2A receptor vasodilation of rat preglomerular microvessels is mediated by EETs that activate the cAMP/PKA pathway. *Am J Physiol Renal Physiol* **291**(1): F155-161.

Chacos N, Capdevila J, Falck JR, Manna S, Martin-Wixtrom C, Gill SS, Hammock BD and Estabrook RW (1983) The reaction of arachidonic acid epoxides (epoxyeicosatrienoic acids) with a cytosolic epoxide hydrolase. *Archives of biochemistry and biophysics* **223**(2): 639-648.

Chou RC, Kim ND, Sadik CD, Seung E, Lan Y, Byrne MH, Haribabu B, Iwakura Y and Luster AD (2010) Lipid-cytokine-chemokine cascade drives neutrophil recruitment in a murine model of inflammatory arthritis. *Immunity* **33**(2): 266-278.

Dai M, Wu L, He Z, Zhang S, Chen C, Xu X, Wang P, Gruzdev A, Zeldin DC and Wang DW (2015) Epoxyeicosatrienoic acids regulate macrophage polarization and prevent LPS-induced cardiac dysfunction. *Journal of cellular physiology* **230**(9):

2108-2119.

Deng Y, Theken KN and Lee CR (2010) Cytochrome P450 epoxygenases, soluble epoxide hydrolase, and the regulation of cardiovascular inflammation. *J Mol Cell Cardiol* **48**(2): 331-341.

Fisher CD, Lickteig AJ, Augustine LM, Ranger-Moore J, Jackson JP, Ferguson SS and Cherrington NJ (2009) Hepatic cytochrome P450 enzyme alterations in humans with progressive stages of nonalcoholic fatty liver disease. *Drug metabolism and disposition: the biological fate of chemicals* **37**(10): 2087-2094.

Gai Z, Gui T, Hiller C and Kullak-Ublick GA (2016) Farnesoid X Receptor Protects against Kidney Injury in Uninephrectomized Obese Mice. *The Journal of biological chemistry* **291**(5): 2397-2411.

Hall Z, Bond NJ, Ashmore T, Sanders F, Ament Z, Wang X, Murray AJ, Bellafante E, Virtue S, Vidal-Puig A, Allison M, Davies SE, Koulman A, Vacca M and Griffin JL (2016) Lipid zonation and phospholipid remodeling in non-alcoholic fatty liver disease. *Hepatology*.

Hu Z, Ren L, Wang C, Liu B and Song G (2012) Effect of chenodeoxycholic acid on fibrosis, inflammation and oxidative stress in kidney in high-fructose-fed Wistar rats. *Kidney & blood pressure research* **36**(1): 85-97.

Imig JD (2012) Epoxides and soluble epoxide hydrolase in cardiovascular physiology. *Physiol Rev* **92**(1): 101-130.

Jiang T, Wang XX, Scherzer P, Wilson P, Tallman J, Takahashi H, Li J, Iwahashi M, Sutherland E, Arend L and Levi M (2007) Farnesoid X receptor modulates renal

Molecular Pharmacology Fast Forward. Published on May 9, 2018 as DOI: 10.1124/mol.117.111047
This article has not been copyedited and formatted. The final version may differ from this version.

lipid metabolism, fibrosis, and diabetic nephropathy. *Diabetes* **56**(10): 2485-2493.

Kim BH, Roh E, Lee HY, Lee IJ, Ahn B, Jung SH, Lee H, Han SB and Kim Y (2008) Benzoxathiole derivative blocks lipopolysaccharide-induced nuclear factor-kappaB activation and nuclear factor-kappaB-regulated gene transcription through inactivating inhibitory kappaB kinase beta. *Molecular pharmacology* **73**(4): 1309-1318.

Lee SM, Schelcher C, Laubender RP, Frose N, Thasler RM, Schiergens TS, Mansmann U and Thasler WE (2014) An algorithm that predicts the viability and the yield of human hepatocytes isolated from remnant liver pieces obtained from liver resections. *PloS one* **9**(10): e107567.

Li P, Oh DY, Bandyopadhyay G, Lagakos WS, Talukdar S, Osborn O, Johnson A, Chung H, Mayoral R, Maris M, Ofrecio JM, Taguchi S, Lu M and Olefsky JM (2015a) LTB4 promotes insulin resistance in obese mice by acting on macrophages, hepatocytes and myocytes. *Nat Med* **21**(3): 239-247.

Li R, Xu X, Chen C, Wang Y, Gruzdev A, Zeldin DC and Wang DW (2015b) CYP2J2 attenuates metabolic dysfunction in diabetic mice by reducing hepatic inflammation via the PPARgamma. *Am J Physiol Endocrinol Metab* **308**(4): E270-282.

Luria A, Bettaieb A, Xi Y, Shieh GJ, Liu HC, Inoue H, Tsai HJ, Imig JD, Haj FG and Hammock BD (2011) Soluble epoxide hydrolase deficiency alters pancreatic islet size and improves glucose homeostasis in a model of insulin resistance.

Proc Natl Acad Sci U S A **108**(22): 9038-9043.

Martinez-Clemente M, Ferre N, Gonzalez-Periz A, Lopez-Parra M, Horrillo R, Titos E, Moran-Salvador E, Miquel R, Arroyo V, Funk CD and Claria J (2010) 5-lipoxygenase deficiency reduces hepatic inflammation and tumor necrosis factor alpha-induced hepatocyte damage in hyperlipidemia-prone ApoE-null mice. *Hepatology* **51**(3): 817-827.

McMahan RH, Wang XX, Cheng LL, Krisko T, Smith M, El Kasmi K, Pruzanski M, Adorini L, Golden-Mason L, Levi M and Rosen HR (2013) Bile acid receptor activation modulates hepatic monocyte activity and improves nonalcoholic fatty liver disease. *The Journal of biological chemistry* **288**(17): 11761-11770.

Miyazaki-Anzai S, Levi M, Kratzer A, Ting TC, Lewis LB and Miyazaki M (2010) Farnesoid X receptor activation prevents the development of vascular calcification in ApoE-/- mice with chronic kidney disease. *Circulation research* **106**(12): 1807-1817.

Needleman P, Turk J, Jakschik BA, Morrison AR and Lefkowith JB (1986) Arachidonic acid metabolism. *Annu Rev Biochem* **55**: 69-102.

Raucy JL, Mueller L, Duan K, Allen SW, Strom S and Lasker JM (2002) Expression and induction of CYP2C P450 enzymes in primary cultures of human hepatocytes. *The Journal of pharmacology and experimental therapeutics* **302**(2): 475-482.

Samuelsson B, Dahlen SE, Lindgren JA, Rouzer CA and Serhan CN (1987) Leukotrienes and lipoxins: structures, biosynthesis, and biological effects.

Science **237**(4819): 1171-1176.

Shitara Y, Hirano M, Sato H and Sugiyama Y (2004) Gemfibrozil and its glucuronide inhibit the organic anion transporting polypeptide 2 (OATP2/OATP1B1:SLC21A6)-mediated hepatic uptake and CYP2C8-mediated metabolism of cerivastatin: analysis of the mechanism of the clinically relevant drug-drug interaction between cerivastatin and gemfibrozil. *The Journal of pharmacology and experimental therapeutics* **311**(1): 228-236.

Sinal CJ, Tohkin M, Miyata M, Ward JM, Lambert G and Gonzalez FJ (2000) Targeted disruption of the nuclear receptor FXR/BAR impairs bile acid and lipid homeostasis. *Cell* **102**(6): 731-744.

Sodhi K, Puri N, Inoue K, Falck JR, Schwartzman ML and Abraham NG (2012) EET agonist prevents adiposity and vascular dysfunction in rats fed a high fat diet via a decrease in Bach 1 and an increase in HO-1 levels. *Prostaglandins Other Lipid Mediat* **98**(3-4): 133-142.

Spector AA and Norris AW (2007) Action of epoxyeicosatrienoic acids on cellular function. *Am J Physiol Cell Physiol* **292**(3): C996-1012.

Spite M, Hellmann J, Tang Y, Mathis SP, Kosuri M, Bhatnagar A, Jala VR and Haribabu B (2011) Deficiency of the leukotriene B4 receptor, BLT-1, protects against systemic insulin resistance in diet-induced obesity. *J Immunol* **187**(4): 1942-1949.

Subbarao K, Jala VR, Mathis S, Suttles J, Zacharias W, Ahamed J, Ali H, Tseng MT and Haribabu B (2004) Role of leukotriene B4 receptors in the development of

atherosclerosis: potential mechanisms. *Arterioscler Thromb Vasc Biol* **24**(2): 369-375.

Tager AM and Luster AD (2003) BLT1 and BLT2: the leukotriene B(4) receptors. *Prostaglandins Leukot Essent Fatty Acids* **69**(2-3): 123-134.

Verbeke L, Mannaerts I, Schierwagen R, Govaere O, Klein S, Vander Elst I, Windmolders P, Farre R, Wenes M, Mazzone M, Nevens F, van Grunsven LA, Trebicka J and Laleman W (2016) FXR agonist obeticholic acid reduces hepatic inflammation and fibrosis in a rat model of toxic cirrhosis. *Sci Rep* **6**: 33453.

Weiss GA, Troxler H, Klinke G, Rogler D, Braegger C and Hersberger M (2013) High levels of anti-inflammatory and pro-resolving lipid mediators lipoxins and resolvins and declining docosahexaenoic acid levels in human milk during the first month of lactation. *Lipids Health Dis* **12**: 89.

Wen X, Wang JS, Backman JT, Kivisto KT and Neuvonen PJ (2001) Gemfibrozil is a potent inhibitor of human cytochrome P450 2C9. *Drug metabolism and disposition: the biological fate of chemicals* **29**(11): 1359-1361.

Xu X, Zhao CX, Wang L, Tu L, Fang X, Zheng C, Edin ML, Zeldin DC and Wang DW (2010) Increased CYP2J3 expression reduces insulin resistance in fructose-treated rats and db/db mice. *Diabetes* **59**(4): 997-1005.

Yang S, Lin L, Chen JX, Lee CR, Seubert JM, Wang Y, Wang H, Chao ZR, Tao DD, Gong JP, Lu ZY, Wang DW and Zeldin DC (2007) Cytochrome P-450 epoxygenases protect endothelial cells from apoptosis induced by tumor necrosis factor-alpha via MAPK and PI3K/Akt signaling pathways. *Am J Physiol*

Heart Circ Physiol **293**(1): H142-151.

Zeldin DC (2001) Epoxygenase pathways of arachidonic acid metabolism. *J Biol Chem* **276**(39): 36059-36062.

Zha W, Edin ML, Vendrov KC, Schuck RN, Lih FB, Jat JL, Bradbury JA, DeGraff LM, Hua K, Tomer KB, Falck JR, Zeldin DC and Lee CR (2014) Functional characterization of cytochrome P450-derived epoxyeicosatrienoic acids in adipogenesis and obesity. *J Lipid Res* **55**(10): 2124-2136.

Zhang S, Wang J, Liu Q and Harnish DC (2009) Farnesoid X receptor agonist WAY-362450 attenuates liver inflammation and fibrosis in murine model of non-alcoholic steatohepatitis. *Journal of hepatology* **51**(2): 380-388.

Molecular Pharmacology Fast Forward. Published on May 9, 2018 as DOI: 10.1124/mol.117.111047
This article has not been copyedited and formatted. The final version may differ from this version.

Footnotes

Conflict of Interest: The authors have no conflict of interest to declare.

Financial Support: This work was supported by the Swiss National Science Foundation [grant # 310030_175639] to Gerd A. Kullak-Ublick and by the "Forschungskredit" of the University Zurich 2015 [grant # FK-15-037] to Zhibo Gai.

Molecular Pharmacology Fast Forward. Published on May 9, 2018 as DOI: 10.1124/mol.117.111047
This article has not been copyedited and formatted. The final version may differ from this version.

Figure legends

Fig. 1. Arachidonic acid metabolism-related gene expression levels in the liver from mice fed a HFD. Scheme of the main arachidonic acid bioactive products **(A)**. Heat-map generated from NGS data of mRNA profiling of genes involved in arachidonic acid metabolism. Blue and red colors indicate downregulation and upregulation in the HFD group, respectively **(B)**. Spearman correlation matrices within the HFD group, between hepatic mRNA expression levels of EET-related enzymes and those of canonical genes involved in inflammation and fibrogenesis **(C)**. CYP2C8 mRNA expression level in liver biopsies from NAFLD and non-NAFLD patients. *n*=5/group. Data are means ± SD, Student's *t* test, *<0.05 **(D)**. CYP2C8 mRNA expression in human liver biopsies and NAFLD score correlation, as determined by histology. Data were normalized for the lowest CYP2C8 mRNA expression value (shown in red) **(E)**.

Fig. 2. Inhibitory effect of OCA on HFD-induced NASH. Serum ALT **(A)**, serum hydroxyproline **(B)**, hepatic NAFLD score **(C)**. Hepatic mRNA levels of mCol1a1 **(D)**, mCcl2 **(E)**, mIcam **(F)**, mTnfa **(G)**, mIl1b **(H)** and mIl6 **(I)**. *n*≥6 mice/group. Data are means ± SD, one-way ANOVA <0.05, Tukey's test, *<0.05. Representative images of immunostaining for the macrophage marker MAC387 **(J)** and CD4 **(K)** in liver sections from chow (a), HFD (b) and HFD+OCA (c) groups.

Molecular Pharmacology Fast Forward. Published on May 9, 2018 as DOI: 10.1124/mol.117.111047
This article has not been copyedited and formatted. The final version may differ from this version.

Fig. 3. Regulatory effect of OCA on arachidonic acid metabolism. Heat-map of mRNA profiling of selected genes involved in arachidonic acid metabolism. The relative expression values of each target gene was measured in the chow, HFD and HFD+OCA mice, normalized for the expression of β-actin and then expressed as HFD:chow (HFD) or HFD+OCA:chow (HFD+OCA) ratio. Each column represents an individual sample. Blue and red colors indicate downregulation and upregulation, respectively **(A)**. Relative hepatic mRNA levels of arachidonate partitioning genes **(B** to **E)**. Serum levels of LTB_4 **(F)** and 14,15-EET **(G)**. Ratio between serum LTB_4 and serum 14,15-EET **(H)**. Urinary levels of 14,15-DHET **(I)**. Data are means ± SD, one-way ANOVA <0.05, Tukey's test, *<0.05. *n*≥6 mice/group.

Fig. 4. Effect of FXR activation on arachidonate metabolism and FFA-induced monocyte migration. Representative images showing crystal violet staining of THP-1 cells onto a 3 μm pore polycarbonate membrane insert upon exposure to the medium of Huh7 cells treated with 50 μM FFA in presence or absence of 2 μM OCA **(A)**. Relative migration score **(B)**. Levels of LTB_4 **(C)**, 14,15-EET **(D)**, LTB_4/14,15-EET ratio **(E)**, and 14,15-DHET **(F)**, in the medium of Huh7 cells exposed to 50 μM FFA in presence or absence of 2 μM OCA. mRNA levels of CYP2C8 in Huh7 cells with the different treatments **(G)**. Data are means ± SD, one-way ANOVA <0.05, Tukey's test, *<0.05. *n*=4/group

Molecular Pharmacology Fast Forward. Published on May 9, 2018 as DOI: 10.1124/mol.117.111047
This article has not been copyedited and formatted. The final version may differ from this version.

Fig. 5. Effect of NF-kB and CYP450 epoxygenase modulation on FFA-induced migration.

Migration score of THP-1 cells in the medium of Huh7 cells treated with 50 μM FFA in combination with 10 μM of the NF-kB inhibitor benzoxathiole derivative (BOT) **(A)** or 20 μM rifampicin **(B)**. Effect of 50 μM FFA on the migration of THP-1 cells in the medium of Huh7 cells transiently overexpressing Cyp2c29 **(C)**. mRNA expression levels of NF-kB target genes in Huh7 cells exposed to 50 μM FFA, 20 μM rifampicin **(D and E**). mRNA expression levels of NF-kB target genes in Huh7 cells transiently overexpressing cyp2c29 and exposed to 50 μM FFA **(F and G)**. Data represents the mean ± SD, one-way ANOVA <0.05, Tukey's test, *<0.05. *n*=3/group.

Fig. 6. Effect of gemfibrozil on OCA-mediated anti-inflammatory action. Representative images showing crystal violet staining of THP-1 cells onto a 3 μm pore polycarbonate membrane insert upon exposure to the medium of Huh7 cells treated with 50 μM FFA in the presence or absence of 2 μM OCA and 100 μM gemfibrozil (GM) **(A)**. Relative migration score **(B)**. Levels of LTB_4 **(C)**, 14,15-EET **(D)** in the medium of Huh7 cells exposed to 50 μM FFA in the presence or absence of 2 μM OCA and 100 μM gemfibrozil (GM).

Fig. 7. Model of the FXR-mediated repression of NF-kB signaling. Increased LTB_4 levels and decreased and EET levels promote NF-κB signaling which triggers hepatic

Molecular Pharmacology Fast Forward. Published on May 9, 2018 as DOI: 10.1124/mol.117.111047
This article has not been copyedited and formatted. The final version may differ from this version.

inflammation **(A)**. Transactivation of cyp450 epoxygenase expression and EET synthesis by FXR, which, in turns, inhibits the NF-κB signaling **(B).**

Molecular Pharmacology Fast Forward. Published on May 9, 2018 as DOI: 10.1124/mol.117.111047
This article has not been copyedited and formatted. The final version may differ from this version.

Table 1. Selected differentially expressed genes in liver from chow mice and HFD mice.

Pathways differentially regulated in HFD-liver
Lipid metabolism
Gpat2 (0.7), Abhd4 (0.6), Acacb (1.2), Acsl5 (0.6), Acsm3 (1.0), Bche (0.7), Echs1 (0.5), Hadh (0.9), Acaca (0.7)
TGFb-induced EMT
TGFb2 (0.8), Jun (1.7), Fos (1.48), Fosl1 (0.8), Mmp2 (1.0), Edn1 (1.4), Vim (0.8), Ocln (-0.8)
Fatty acid metabolism
Cd74 (1.5), Elovl5 (1.6), Aacs (2.0), Acaa1b (1.3), Acacb (1.2), Acsf3 (0.7), Acsl5 (0.6), Acsm3 (1.0), Ch25h (1.3), Elovl2 (0.9), Echs1 (0.5), Fads1 (0.8), Fads2 (1.3), Fasn (1.5), Gpam (0.9), Hao2 (3.0), Hadh (0.9), Hsd17b4 (0.5), Myo5a (1.0), Elovl6 (0.9), Acaca (0.7), Scd1 (1.6), Scd2 (1.0), Scd3 (1.5)
Arachidonic acid metabolism
Cbr3 (1.6), Pla2g6 (0.9), Cyp2c29 (-1.2), Cyp2c37 (-0.8), Cyp2c39 (-0.7), Cyp2c44 (-1.0), Cyp2c50 (-0.7), Cyp2c54 (-1.2), Cyp2c55 (-1.3), Cyp2c70 (-1.6), Cyp4f14 (-0.7)

Numbers in parentheses indicate gene expression levels quantified as log2 of fold changes.

Molecular Pharmacology Fast Forward. Published on May 9, 2018 as DOI: 10.1124/mol.117.111047
This article has not been copyedited and formatted. The final version may differ from this version.

Fig 1

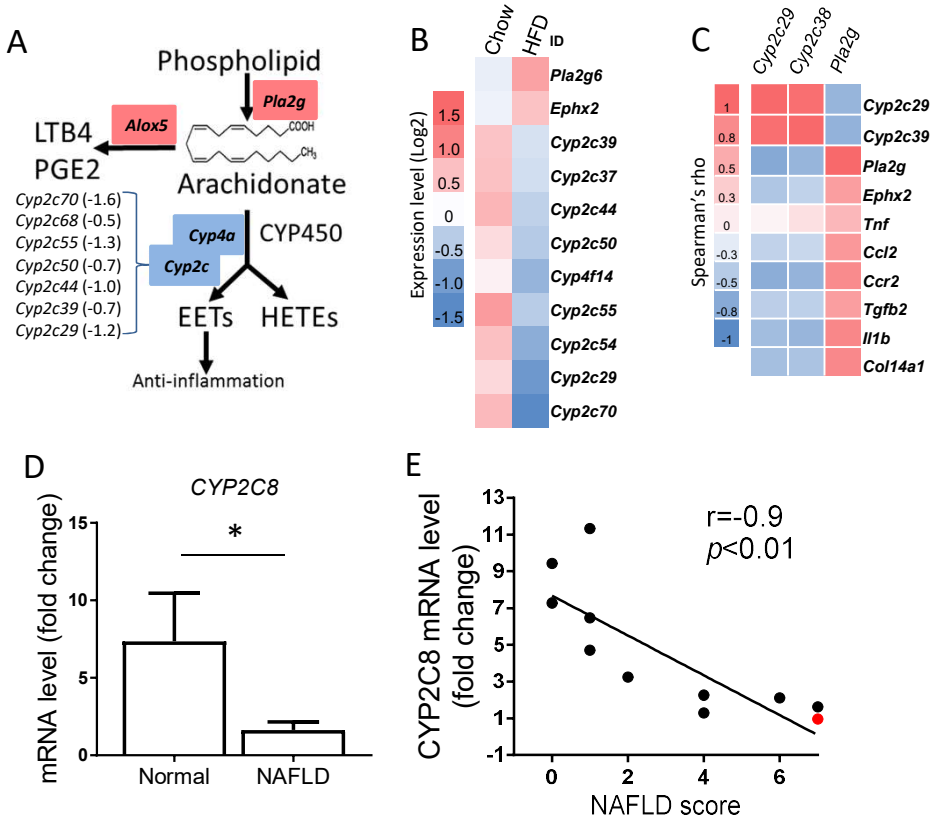

Molecular Pharmacology Fast Forward. Published on May 9, 2018 as DOI: 10.1124/mol.117.111047
This article has not been copyedited and formatted. The final version may differ from this version.

Fig 2

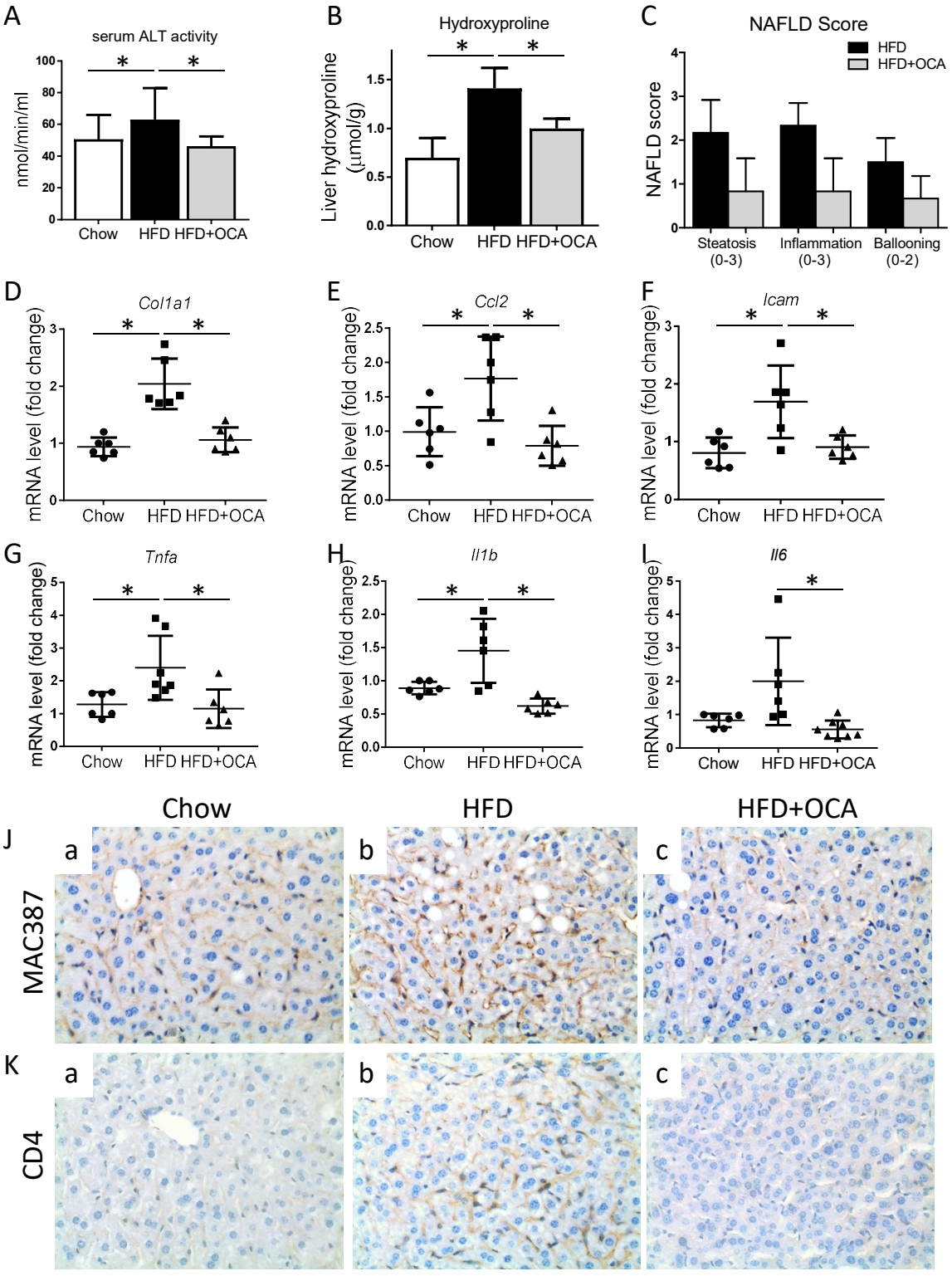

Molecular Pharmacology Fast Forward. Published on May 9, 2018 as DOI: 10.1124/mol.117.111047
This article has not been copyedited and formatted. The final version may differ from this version.

Fig 3

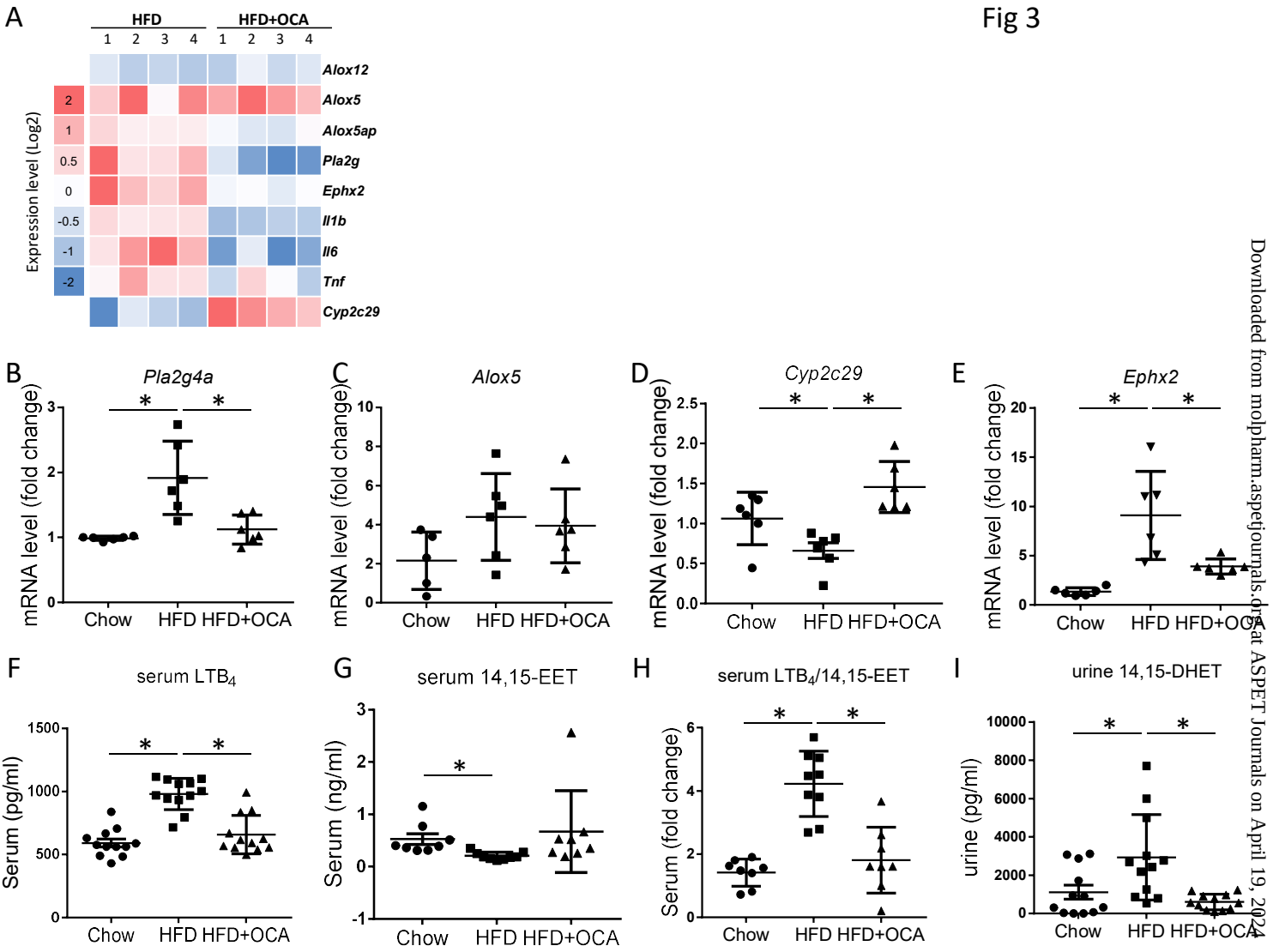

Molecular Pharmacology Fast Forward. Published on May 9, 2018 as DOI: 10.1124/mol.117.111047
This article has not been copyedited and formatted. The final version may differ from this version.

Fig 4

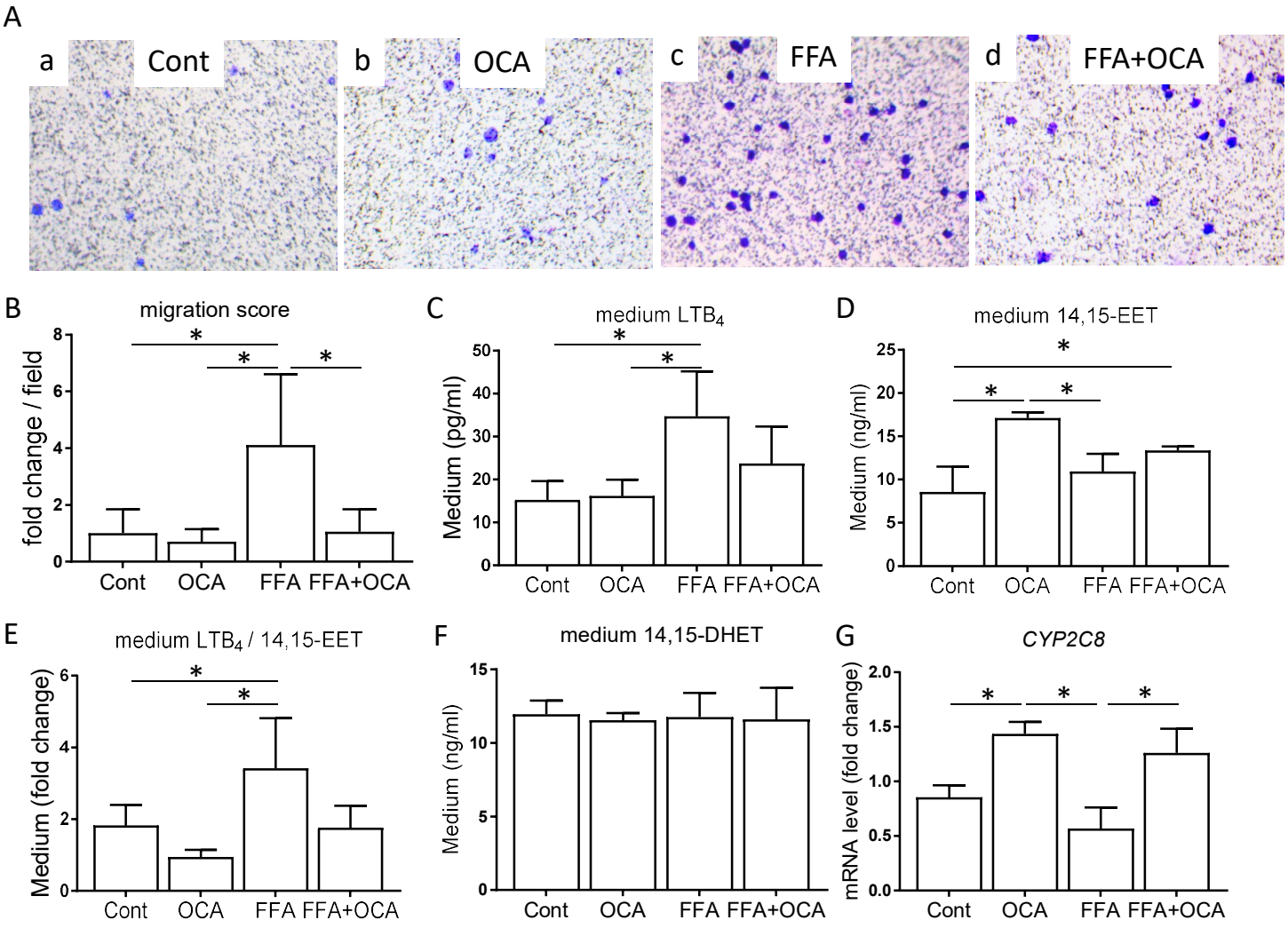

Molecular Pharmacology Fast Forward. Published on May 9, 2018 as DOI: 10.1124/mol.117.111047
This article has not been copyedited and formatted. The final version may differ from this version.

Fig 5

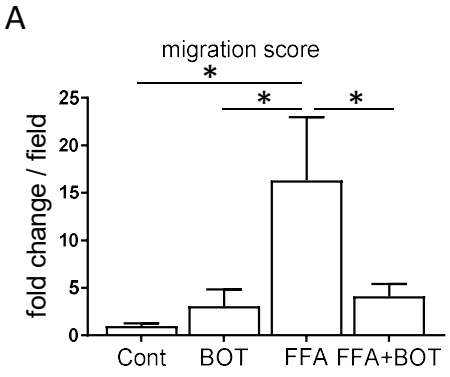

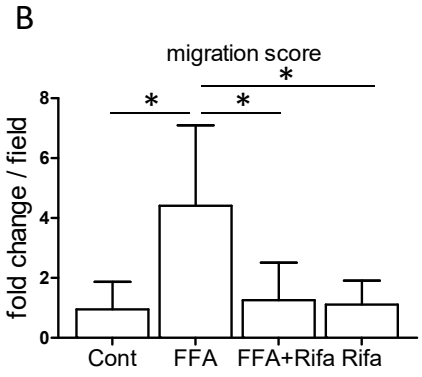

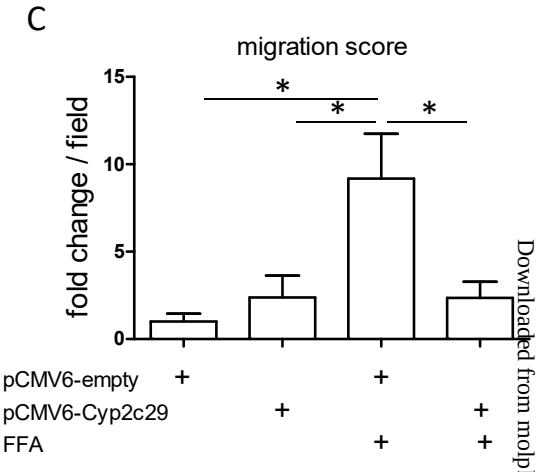

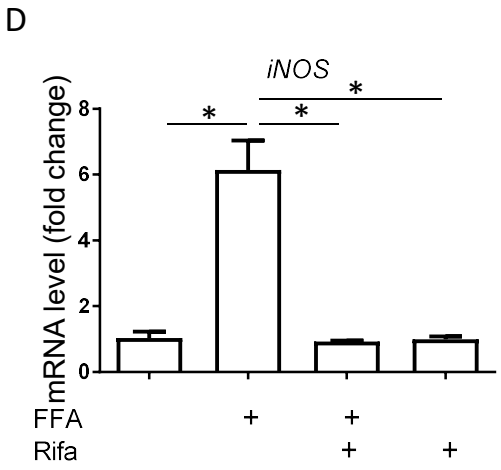

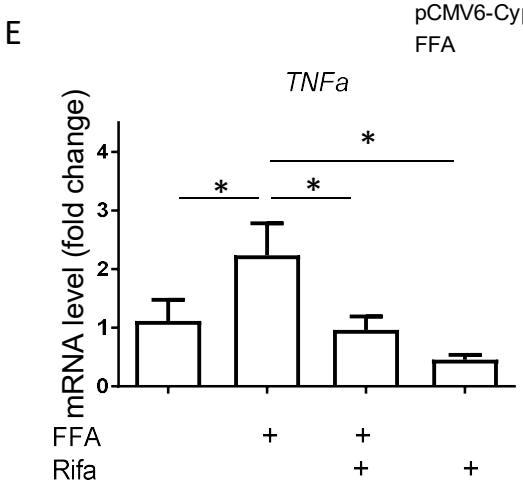

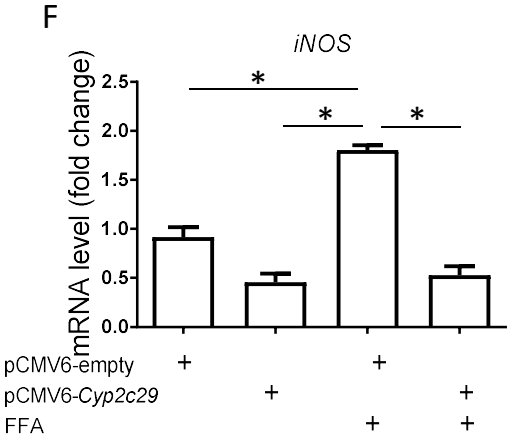

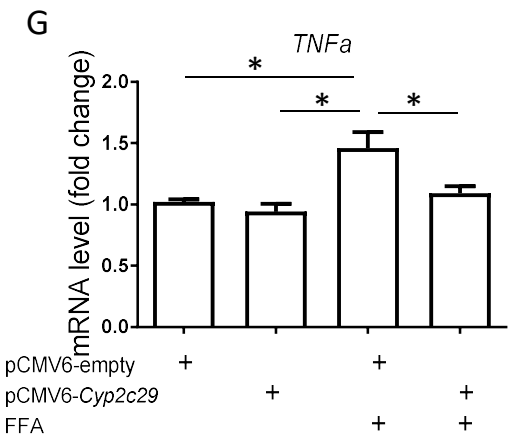

Molecular Pharmacology Fast Forward. Published on May 9, 2018 as DOI: 10.1124/mol.117.111047
This article has not been copyedited and formatted. The final version may differ from this version.

Fig 6

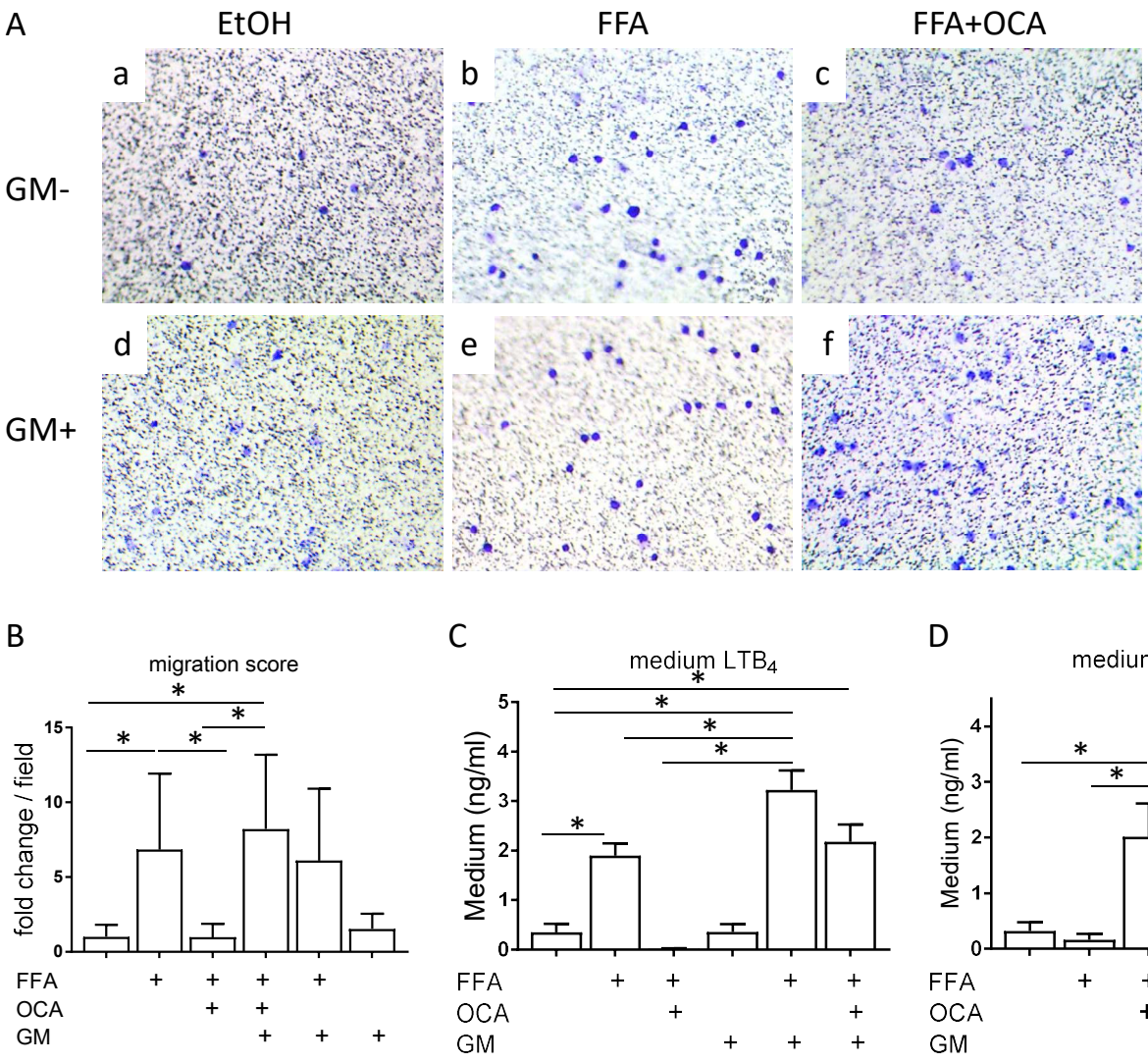

Molecular Pharmacology Fast Forward. Published on May 9, 2018 as DOI: 10.1124/mol.117.111047
This article has not been copyedited and formatted. The final version may differ from this version.

Fig 7

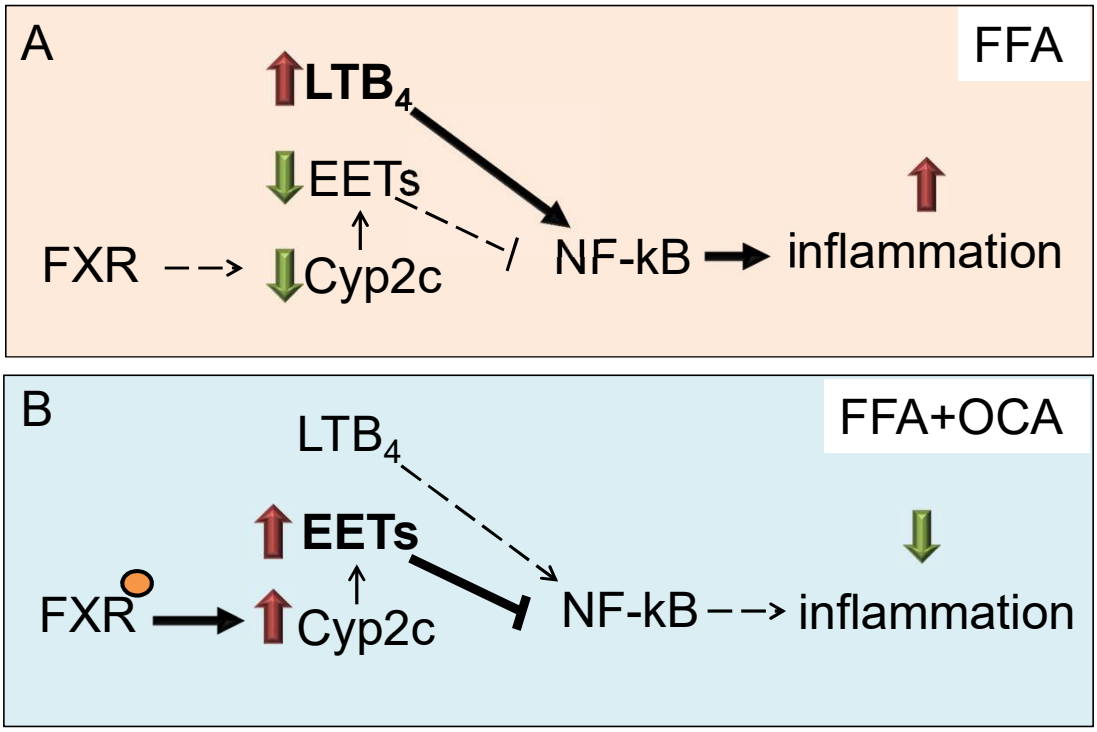

The effects of farnesoid X receptor activation on arachidonic acid metabolism, NF-kB signaling and hepatic inflammation

Zhibo Gai, Michele Visentin, Ting Gui, Lin Zhao, Wolfgang E. Thasler, Stephanie Häusler, Ivan Hartling, Alessio Cremonesi, Christian Hiller and Gerd A. Kullak-Ublick

Molecular Pharmacology

Results

Supplementary Fig. 1. NASH assessment in mice fed a HFD.

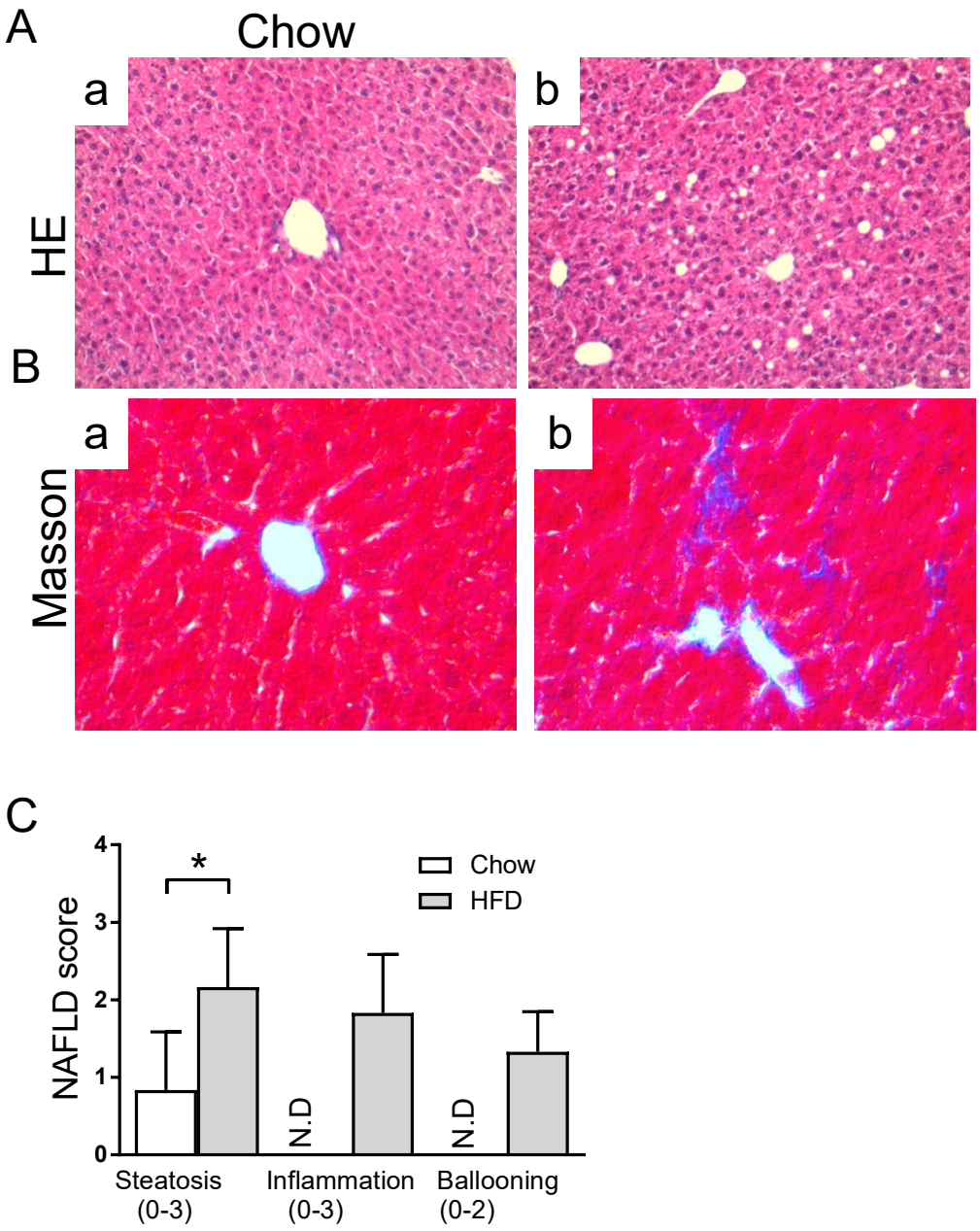

Representative images of hematoxylin-eosin **(A)** and Masson **(B)** staining in liver sections from chow and HFD groups. NAFLD score, *n*=6 mice/group. Data are the means ± SD, Student's *t* test, *<0.05 **(C)**.

Supplementary Fig. 2. Arachidonic acid metabolism in mice fed a HFD.

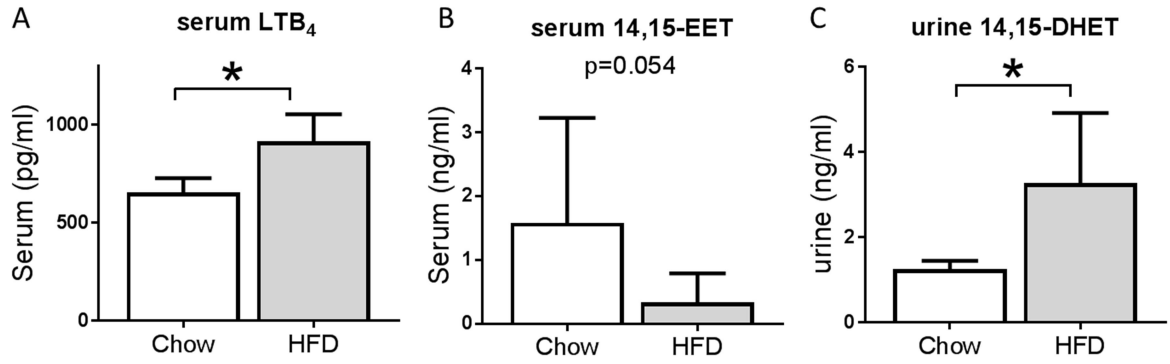

Serum levels of LTB_4 **(A)** and 14,15-EET **(B)**. Urine levels of 14,15-DHET **(C)**. *n*=6 mice/group. means ± SD, Student's *t* test, *<0.05.

Supplementary Fig. 3. Effect of OCA on HFD-induced NASH.

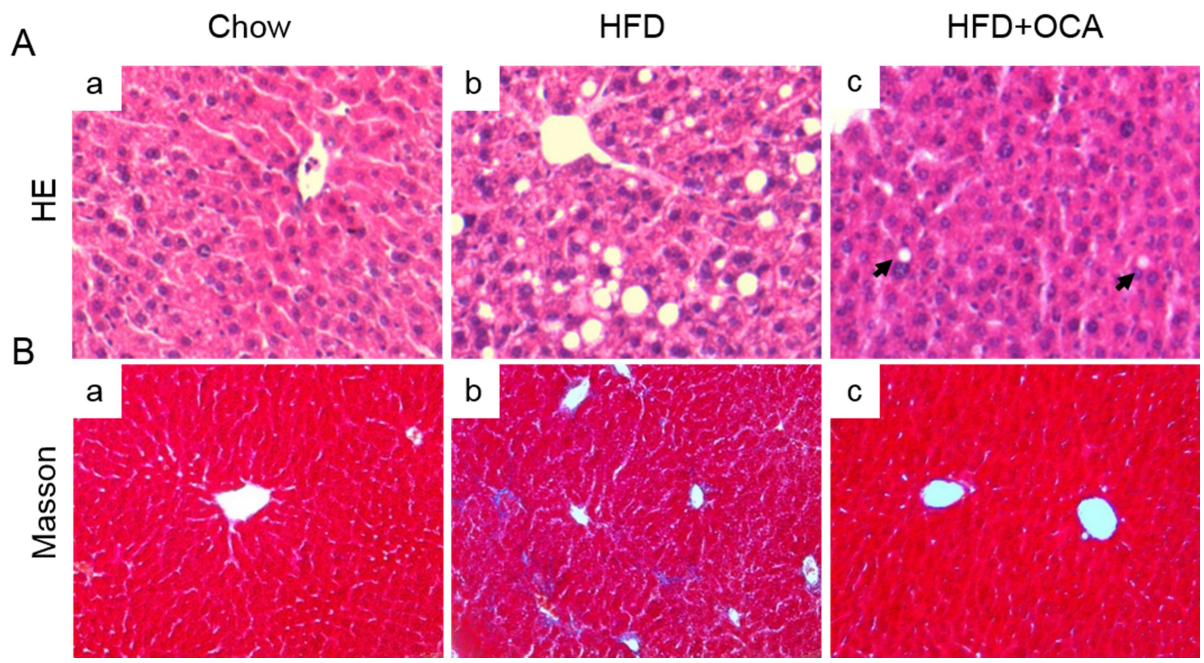

Representative images of hematoxylin-eosin **(A)** and Masson **(B)** staining in liver sections from chow (a), HFD (b) and HFD+OCA groups (c).

Supplementary Fig. 4. Effect of OCA on the expression of FXR target genes in Huh7 cells.

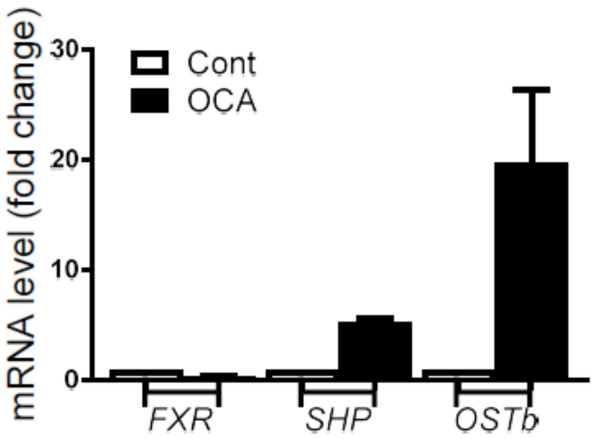

mRNA expression levels of FXR, SHP and OSTb in Huh7 cells exposed for 24h to OCA at the extracellular concentration of 2 μM. *n*=3 /group. Data are means ± SD.

Supplementary Fig. 5. Impact of FXR activation on FFA-induced monocyte migration and EET metabolism-related gene expression levels in primary cultured hepatocytes from mouse (A and B) and human (C and D).

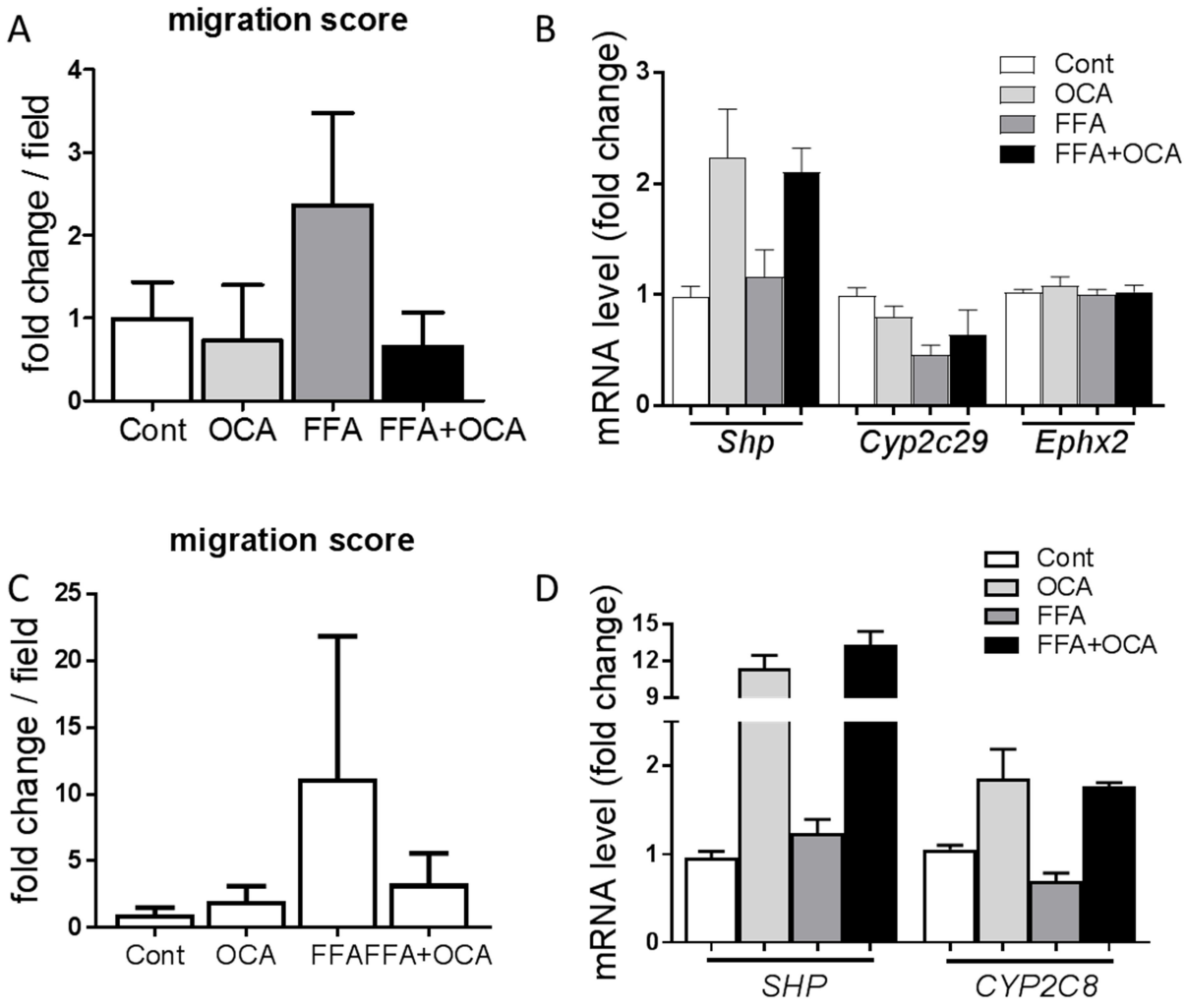

Migration score of J774 cells **(A)** and mRNA expression levels of Shp, Cyp2c29 and Ephx2 in primary cultured hepatocytes treated for 48h with the indicated conditions. *n*=3/group **(B)**. Migration score of THP-1 cells **(C)** and mRNA expression levels of SHP and CYP2C8 in primary cultured human hepatocytes treated for 48h with the indicated conditions. Data represents the mean±SD from 3 technical replicate of one donor **(D)**.

Supplementary Fig. 6. Effect of the co-incubation with OCA and the FXR antagonist z-Guggulsterone (Gu) on FXR activation and FFA-induced monocyte migration.

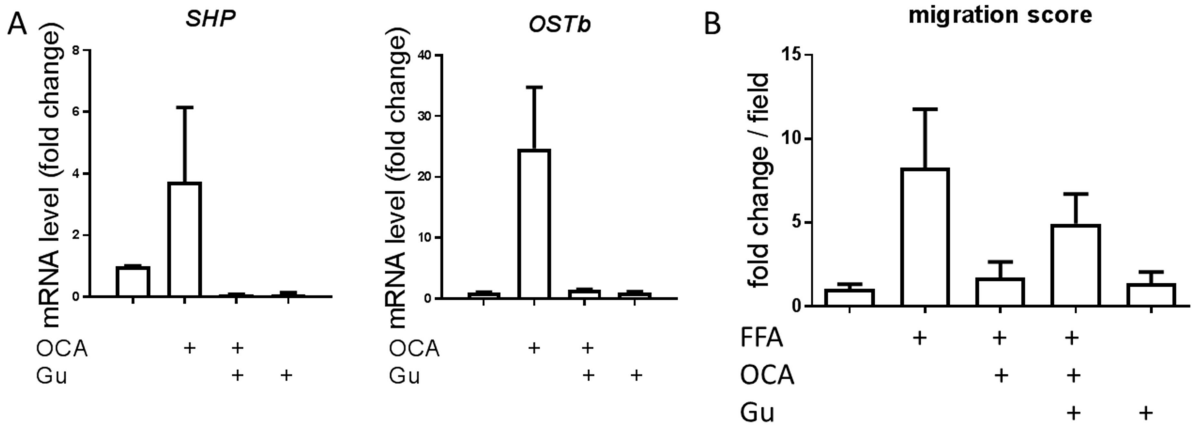

mRNA expression levels of SHP and OSTb and in Huh7 cells co-exposed for 48h to OCA (2 μM) and Gu (25μM) **(A)**. Migration score of monocyte-like J773 cells at the indicated conditions. *n*=2/group **(B)**. Data are expressed as means ± SD.

Supplementary Fig. 7. Effect of OCA, Gemfibrozil (GM) or Rifampicin (Rifa) on THP-1 cell migration induced by serum or exogenous LTB_4.

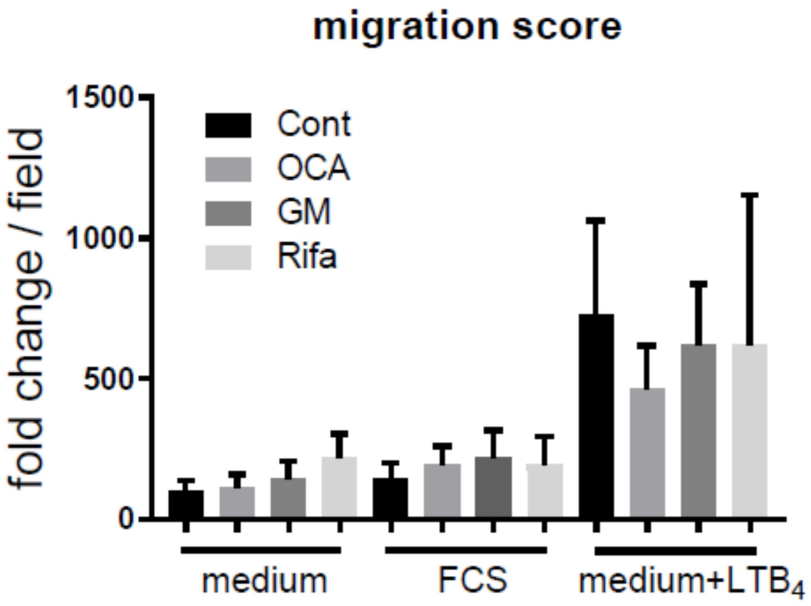

Migration score of THP-1 cells exposed for 48h with the indicated conditions. *n*=3/group. Data represents the mean±SD from 3 independent experiments.